



Citation for published version:

Vats, G, Ravikant, Kumari, S, Pradhan, D, Katiyar, R, Ojha, VN, Bowen, C & Kumar, A 2019, 'Magnetocaloric effect and piezoresponse of engineered ferroelectric-ferromagnetic heterostructures', *Journal of Magnetism and Magnetic Materials*, vol. 473, pp. 511-516. <https://doi.org/10.1016/j.jmmm.2018.10.024>

DOI:

[10.1016/j.jmmm.2018.10.024](https://doi.org/10.1016/j.jmmm.2018.10.024)

Publication date:

2019

Document Version

Peer reviewed version

[Link to publication](#)

Publisher Rights

CC BY-NC-ND

University of Bath

General rights

Copyright and moral rights for the publications made accessible in the public portal are retained by the authors and/or other copyright owners and it is a condition of accessing publications that users recognise and abide by the legal requirements associated with these rights.

Take down policy

If you believe that this document breaches copyright please contact us providing details, and we will remove access to the work immediately and investigate your claim.

Magnetocaloric effect and piezoresponse of engineered ferroelectric-ferromagnetic heterostructures

Gaurav Vats^{a, #, *}, Ravikant^{b, #}, Shalini Kumari^c, Dhiren K Pradhan^d, Ram S Katiyar^e, V. N. Ojha^b,
Chris R Bowen^f, Ashok Kumar^{b, *}

^a*School of Materials Science and Engineering, University of New South Wales, Sydney 2052, Australia*

^b*CSIR-National Physical Laboratory, Dr. K. S. Krishnan Marg, Delhi, 110012, India*

^c*Department of Physics and Astronomy, West Virginia University, Morgantown, WV 26506, USA*

^d*Extreme Materials Initiative, Geophysical Laboratory, Carnegie Institution for Science, Washington, DC 20015, USA*

^e*Department of Physics and Institute for Functional Nanomaterials, University of Puerto Rico, San Juan, PR 00931-3343, USA*

^f*Materials Research Centre, Department of Mechanical Engineering, University of Bath, Bath BA2 7AY, United Kingdom*

***Email:** er.gauravvats17@gmail.com, ashok553@nplindia.org ; **Phone:** +61-481354339

Authors contributed equally.

Abstract:

Present study reports the magnetocaloric effect (MCE) and piezoresponse of integrated ferroelectric-ferromagnetic heterostructures of $\text{PbZr}_{0.52}\text{Ti}_{0.48}\text{O}_3$ (PZT) (5 nm)/ $\text{Bi-Sr-Ca-Cu}_2\text{-O}_x$ (BSCCO) (5 nm)/ $\text{La}_{0.67}\text{Sr}_{0.33}\text{MnO}_3$ (LSMO) (40 nm)/ MgO. Magnetic and piezoresponse behavior of the heterostructures are found to be governed by magneto-electric coupling and induced lattice strains. In addition, the MCE is studied using Maxwell equations from both Field Cooled (FC) and Zero Field Cooled (ZFC) magnetization data. Maximum MCE entropy change ($|\Delta S|$) of $42.6 \text{ mJkg}^{-1}\text{K}^{-1}$ (at 258 K) and $41.7 \text{ mJkg}^{-1}\text{K}^{-1}$ (at 269 K) are found corresponding to FC and ZFC data, respectively. The variation in maximum entropy change and corresponding temperatures for FC and ZFC data revealed that the application of a magnetic field can significantly contribute towards tuning of the MCE. Interestingly, these multilayered structures are found to sustain MCE over a broad temperature range, which makes them attractive for improved solid-state energy conversion devices.

Keywords: Magnetocaloric effect; Magneto-electric coupling; Lattice strains; Multi-layered heterostructures.

1. Introduction

Adiabatic tuning of magnetization leading to an isothermal entropy/heat change is popularly known as the *magneto-caloric effect* (MCE) [1]. The effect was primarily exploited for laboratory applications[2], until the “giant” (at least 2 times higher in existing similar magnetic materials) MCE was discovered using reversible distortions in symmetry[1, 3-8] or volume[9], aided by strongly coupled magnetic and structural transitions[10]. This approach attracted significant research interest in terms of exploring different classes of materials for tuning and achieving a giant MCE. Among these materials, gadolinium has proven to be a strong candidate for MCE refrigeration and is often considered as a reference material to benchmark a MCE[11]. However, a high cost has hindered the development of commercial devices based on gadolinium. In this context, semi-metallic perovskite lanthanum manganite ($\text{La}_{0.7}\text{Sr}_{0.3}\text{MnO}_3$; LSMO)[12-14] based compositions have attracted renewed interest, primarily after the discovery of a colossal magnetoresistance in doped lanthanum manganite thin films[15, 16]. Thin films with a range of compositions and configurations have been extensively studied to provide an improved alternative for gadolinium[11, 17-25]. Efforts have been made to tune the MCE by employing different synthesis techniques[18, 20]. In addition, work has been done to enhance the MCE performance of LMSO by doping of the La and Mn sites[17, 19, 26].

It has been reported that during cooling LSMO exhibits a paramagnetic (PM) to ferromagnetic (FM) transitions above room temperature (369 K)[17]. These transitions can be tuned using chromium (Cr) and titanium (Ti) substitution at temperatures of 326 K and 210 K, respectively[27]. The change in the thickness of LSMO layer can also act to tune of these transition temperatures[28]. Compositional and configurational tuning also leads to variation in magnetization dependant heat capacity which further affects its magnetocaloric cooling capacity;

as an example, the magnetization dependent change in heat capacity ($\Delta C_P(T, \mu_0 H) = C_P(T, \mu_0 H) - C_P(T, 0)$) of Ti-substituted LSMO ranges for 6.2 to -4.2 $\text{Jkg}^{-1}\text{K}^{-1}$ while for Cr substituted compositions it lies in the range of 21 to -11 $\text{Jkg}^{-1}\text{K}^{-1}$ [27]. This huge variation in heat capacity is a reason why Ti-substituted compositions exhibit a better MCE. LSMO thin films have been grown on a variety of substrates, and the epitaxial strain has been utilized to enhance the MCE performance of LSMO[25]. Intriguingly, attempts to improve MCE performance by growing $\text{La}_{0.7}\text{Sr}_{0.3}\text{MnO}_3/\text{SrRuO}_3$ (LSMO/SRO) superlattices have led to improved relative cooling capacity as a result of broadening of the range of maximum temperature change with a small deviation in MCE entropy[24, 29]. This highlighted the potential benefits of interlayer coupling and interface effects[24, 29]. Similar observations are also evident from the recent demonstration of pyroelectric control of magnetization for enhanced MCE performance in ferroelectric-ferromagnetic multi-layered heterostructures[30]. This work unfurls the importance of ferroelectric-ferromagnetic coupling for realization of significant MCE efficiency. In this work, a 70 nm CoFe_2O_4 layer was sandwiched between two 270 nm Zr-doped lead titanate (PZT) layers. Due to this the pyroelectric effect in PZT layers predominantly governed the magnetization of the system. It is to be noted that PZT layers exhibit good ferroelectricity down to 2.4 nm [28]. Therefore, it has attained huge research interests for ultra-thin film applications such as ferroelectric tunnel junctions [28, 31-33]. Moreover, it has been reported that a very thin (5-7 nm) PZT capping layer on LSMO (30 nm thick) results in improved magnetic response[28, 34]. It is important to note that a superconducting spacer between ferroelectric and ferromagnetic may capitalize the quanta of magnetic flux and couple the local ferroelectric polarization with local magnetization at nanoscale[35]. As a result of these observations, we have investigated PZT/BSCCO/LSMO/MgO ($\text{PbZr}_{0.52}\text{Ti}_{0.48}\text{O}_3$ (PZT) (5 nm)/ Bi-Sr-Ca-Cu₂-O_x (BSCCO) (5 nm)/

$\text{La}_{0.67}\text{Sr}_{0.33}\text{MnO}_3$ (LSMO) 40nm/ MgO) heterostructures as a ferroelectric-ferromagnetic configuration with a superconducting spacer to achieve an improved magnetic response. It is of interest to note that a thin layer of superconducting spacer BSCCO cannot exhibit superconductivity above 100 K, as also evident from the zero-field cooled magnetic data of the heterostructure but it is still likely to facilitate the ferroelectric-ferromagnetic coupling[36]. The MCE in the present case is governed by the cumulative effect of epitaxial lattice strains and magnetoelectric coupling.

2. Experiments

Targets of the superconducting Bi-Sr-Ca-Cu₂-O_x (BSCCO) and ferroelectric $\text{Pb}(\text{Zr}_{0.52}\text{Ti}_{0.48})\text{O}_3$ (PZT) were synthesized by the conventional solid-state reaction route. Stoichiometric ratios of high-quality precursors (>99.9%, Sigma Aldrich) of Bi_2O_3 , SrCO_3 , CaCO_3 , CuO and PbO , ZrO_2 , TiO_2 were used to synthesize BSCCO and PZT targets, respectively. The powders were well mixed and ground in an isopropyl alcohol medium using a mortar-pestle for two hours to form a homogeneous mixture of the precursor. The fine ground powder was calcined at 850 °C for BSCCO and 800 °C for PZT, respectively. Afterward, the phase pure calcined powders were pelletized into 25.4 mm (one-inch) circular shaped targets and sintered for four hours at 860 °C and 1200 °C for the BSCCO and PZT, respectively. The superconductivity of BSCCO target was confirmed by the levitation and measurement of resistance with temperature.

After forming the targets, multilayer nanostructures of BSCCO, PZT and LSMO thin films on a MgO (001) substrate were fabricated using a Pulsed Laser Deposition (PLD) technique. A multi-target mounting PLD system was used to grow alternate layers without breaking the vacuum. Both target and substrate holders were rotated to maintain the homogeneity of the thin films.

Initially, the PLD chamber was evacuated to a sufficiently low pressure ($\sim 1.2 \times 10^{-6}$ torr) to avoid any residual gas contamination during the growth process. Firstly, the LSMO layer was deposited on the MgO (001) substrate using an Excimer laser ($\lambda = 248$ nm) with an energy density of 1.5-2 J/cm² at 780 °C with a repetition rate of 5 Hz and an oxygen partial pressure of 100 mT. Subsequently, an ultra-thin layer (~ 5 nm) of BSCCO was grown on the LSMO/MgO substrate under similar conditions followed by the deposition of an ultra-thin PZT (~ 5 nm) layer under similar conditions for polar capping. The thickness of films was measured using *Stylus Profiler*. The ferroelectric /ferromagnetic heterostructure was finally annealed at 700 °C for 30 minutes to improve the interface and crystalline properties. Structural characterization was performed using X-ray diffraction technique (Bruker Advance) with CuK α radiation (1.54 Å).

Analysis of the surface topography and piezoresponse force microscopy was carried out at room temperature with moderately stiff ($k \sim 1$ N/m) Budget Sensors ElectriMulti 75-G cantilevers having a free resonance of ~ 75 kHz, on a Multimode (Veeco) AFM equipped with a Nanonis controller. Cryogenic magnetic measurements were performed using the Quantum designed Physical Property Measurement System (PPMS) in the temperature range of 100 K to 330 K and applied magnetic field ranges from 0 to 2.0 Tesla. However, an appropriate magnetic response is observed only at very low applied magnetic fields (< 0.1 T). These measurements indicated that the deposited heterostructures demonstrate a large difference in magnetization with respect to the change in temperature ($\partial M / \partial T$) with low hysteresis losses, which makes these heterostructures of interest for energy efficient MCE investigations.

3. Results and Discussion

3.1 Crystal structure, Surface Topography & Piezoresponse Force Microscopy (PFM) Study:

Typical θ - 2θ X-ray diffraction patterns of the $\text{PbZr}_{0.52}\text{Ti}_{0.48}\text{O}_3$ (PZT) (5 nm)/ $\text{Bi-Sr-Ca-Cu}_2\text{-O}_x$ (BSCCO) (5 nm)/ $\text{La}_{0.67}\text{Sr}_{0.33}\text{MnO}_3$ (LSMO) 40nm/ MgO heterostructure was recorded in the 20° to 80° range of Bragg's angle; see Figure 1. The hkl planes of the LSMO, PZT, and BSCCO were observed in the direction of the MgO (001) substrate which provides evidence of preferential orientation during growth. The growth direction of the heterostructure is along the c-axis and is perpendicular to the substrate plane. The bulk polycrystalline LSMO ceramic is a distorted perovskite with a pseudo-cubic lattice parameter $a = c = 3.872 \text{ \AA}$, whereas tetragonal bulk PZT shows $a = 4.033 \text{ \AA}$ $c = 3.141 \text{ \AA}$. The hkl planes of the LSMO thin film are found at 22.9° , 46.74° , 73.08° , a mismatch in substrate and film lattice parameters confirms the presence of an in-plane tensile strain and out of plane compressive strain. The literature suggests that the magnetization and isothermal entropy change can be significantly influenced by introducing such epitaxial strains[25] as a result of the growth process, which can be calculated using the relation;

$$\epsilon = \frac{a_{\text{film}} - a_{\text{bulk}}}{a_{\text{bulk}}} \quad (1)$$

where a_{bulk} is the lattice constant of the bulk polycrystalline PZT and LSMO ceramic used as target for PLD technique and a_{film} is the lattice constant of the grown thin film obtained from XRD data. The lattice constants of PZT and LSMO thin films obtained from XRD data are $c = 3.889 \text{ \AA}$ and $c = 4.093 \text{ \AA}$, respectively. The LSMO thin film, when grown on the MgO (001) substrate and PZT on the smooth BSCCO/LSMO/MgO possess in-plane tensile strain of +0.42 % and in-plane compressive strain of -1.16 %, respectively. This leads to the generation of an in-plane tensile strain in the LSMO layer and a compressive strain in the BSCCO thin film; it is

well known that a lattice strain significantly alters the magnetic properties of thin films due to piezo- magnetostriction[37, 38].

Following structural characterization, the surface topography was investigated using atomic force microscopy (AFM), performed using a platinum coated (Pt/Si) cantilever tip. The nanoscale ferroelectric and piezoelectric nature of the PZT layer was investigated with the aid of piezoresponse force microscopy (PFM), as shown in Figure 2 (a-d). The heterostructures were found to have a homogeneous surface with a nanoscale granular structure on the upper surface. These may be due to the presence of the thin nanostructured layer of BSCCO beneath the PZT layer. It is also possible that granular structure on the top of heterostructure may arise due to non-uniform Stranski–Krastanov (SK) growth mechanism of PZT on BSCCO/LSMO/MgO heterostructure [39, 40]. Repeated PFM measurements at different locations revealed significant point-to-point variability of the local coercive voltage[41-43], Figure 2 (b) shows the polarization switching with electric poling of the upper surface using external 8 V DC bias where a polarization reversal signature under a DC bias was observed. However, a complete reversal of polarization was missing. The phase angle shows a square hysteresis with 180 degree phase reversal, with average coercive voltage of less than 3.5 V. An in-built electric field is present in the heterostructure due to strain present in the piezoelectric PZT layer or domain pinning. The minima of the amplitude loop indicate that the local coercive voltages are nearly +5.0 V and -5.0 V; see Figure 2 d. These coercive fields vary point-to-point, depending on the distribution of ferroelectric domain and its pinning by various defects and an interfacial dead layer. The properties of phase reversal, polarization switching, domain distribution, and domain pinning depend on the depolarization effect, which is common in ultra-thin films close to the critical thickness.

3.2 Magneto-Caloric Effect (MCE)

Maxwell relations[44] suggests that the MCE entropy change (ΔS_M) for an applied magnetic field (H) can be estimated as,

$$\Delta S_M = \int_{T_1}^{T_2} \left(\frac{\partial M}{\partial T} \right)_H dT \quad (2)$$

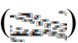
where μ_0 is the permeability of the free space. The $\left(\frac{\partial M}{\partial T} \right)_H$ can be obtained through a set of $M(H)$ isotherms obtained from thermodynamic equilibrium. In addition, the corresponding MCE temperature change (ΔT) can be determined by the following equation,

$$\Delta T = \frac{\Delta S_M}{C} \quad (3)$$

where C is the specific heat capacity of the material and can be assumed constant in the absence of phase transitions. To investigate the MCE, the isothermal magnetization $M(T)$ data of the PZT/BSCCO/LSMO/MgO heterostructures were recorded in the Zero Field Cooled (ZFC) and Field Cooled (FC) modes using the standard protocol[10]. Both ZFC and FC, $M(T)$ measurements were performed in the temperature range of 100 K to 330 K with the interval of 1 K, where the applied magnetic field $\mu_0 H$ was varied from 0 T to 0.1 T, as shown in figure 3 (a) and (b). It is to be noted that the magnetization hysteresis loops were obtained for -0.1 to 0.1 T, while the measurements are performed for 0 to 0.1 T. This is because the complete $M-H$ curve forms a hysteretic system and thermodynamics cannot be applied to them[45]. Therefore, for adequate usage of Maxwell relations, the estimates can be performed either in the first or third quadrant of the $M-H$ curve[45]. However, estimates from both the first or third quadrants will lead to the same results. Figure 3 shows that the magnetization slowly decreases near to the ferromagnetic (FM) phase transition; however, the magnetic moment falls to zero at the

ferromagnetic to paramagnetic (PM) transition. The maximum value of magnetization for the heterostructures is found significantly higher in comparison the maximum magnetization values reported for various LSMO based composition and heterostructures[17-25]. This is due to the cumulative effect of the presence of BSCCO and PZT. BSCCO help in facilitating electromagnetic coupling while PZT capping layer leads to a better magnetic response. LSMO thin films are known to demonstrate magnetostriction (an effect where a change in magnetization leads to a change in the shape of the material)[46, 47]. This indeed lead to a converse piezoelectric effect in the adjacent piezoelectric layer where the polarization of material is changed due to change in induced strain by magnetostriction of LSMO. These induced strains cause a change in polarization of PZT by displacement of the central atom (Zr/Ti). This displacement of the central atom induces an electric field which further leads to change in overall magnetization of the system. Another important observation is reduced Curie temperature (T_m) of the grown heterostructures in contrast to the LSMO thin films. Various studies suggest that the LSMO thin film exhibits phase transition at $T_m \sim 330$ K; however in the present study the T_m is shifted to ~ 300 K due to magnetoelectric coupling and a compressive strain present in PZT/BSCCO capping layer[23]. In addition, a small difference in FC and ZFC data is observed (Figures 3 (c)-(f)). This could be due to the variation in strain that affects alignment of magnetic domains during FC and ZFC measurements. Another possible reason is the trigger mechanism of the converse piezoelectric effect in the PZT layer. It is obvious that during a FC measurement there will a significant change in in-plane magnetization of LSMO in contrast to ZFC measurement. Therefore, the impact of the out of plane induced electric field on PZT layer will be different, resulting in variation of additional lattice strains due to induced electric field by converse piezoelectric effect. These strains are difficult to be measured/predicted due to the

complexity of the coupling, and equation 1 does not account for them. But the confirmation of an excellent piezoelectric response of PZT at room temperature (in the vicinity of LSMO magnetic transition temperature in the present case (300 K)) in our films strongly supports this hypothesis. The in-plane tensile strain calculated using equation 1, in LSMO films with an upper layer of compressively strained PZT considerably affects the magnetic dipole alignment during FC and ZFC measurement and therefore the maximum change in the isothermal entropy; this significantly affects the cooling capacity of the heterostructures. Theoretical and experimental studies have proven that strain in thin films also affects the Curie temperature (T_m)[48], since T_m is ~ 300 K in the heterostructure and is at least 30 K lower than the bulk LSMO. The strain present in the various layers of the heterostructure and presence of BSCCO layer influences the magnetization which leads to significant entropy change even at low applied field (< 0.1 T) and over a broad temperature spectrum resulting in a MCE temperature change (ΔT).

The variation in the temperature dependent isothermal magnetic entropy () of the PZT/BSCCO/LSMO/MgO heterostructure is calculated from the in-plane magnetization $M(H)$ in the vicinity of ferromagnetic phase transition temperature, namely 150 K to 330 K. The MCE entropy (ΔS) and temperature change (ΔT), estimated using equations 1 and 2 are highlighted in Figure 4, respectively (using $\rho = 8.3 \text{ gcm}^{-3}$ and $C = 330 \text{ JK}^{-1}\text{kg}^{-1}$ which are assumed constant with temperature as the heterostructures are investigated below 1 T)[30, 49]. Any magnetic material possesses a maximum change in its isothermal magnetic entropy near the magnetic phase transition where the degree of magnetization changes significantly. In the present case, the effect is governed by magneto-electric coupling and induced lattice strains. The PZT/BSCCO/LSMO/MgO heterostructures are found to have maximum entropy change ($|\Delta S|$) of $42.6 \text{ mJkg}^{-1}\text{K}^{-1}$ at 258 K and $41.7 \text{ mJkg}^{-1}\text{K}^{-1}$ at 269 K, which correspond to FC and ZFC

magnetization measurements in an applied magnetic field ($\mu_0\Delta H$) range of 0.1 T, respectively. The variation in maximum entropy change and corresponding temperatures for FC and ZFC data reveals that applying a magnetic field can significantly contribute towards tuning of the MCE, see Figure 4 (a) and (b). The same trend could also be observed in the MCE temperature change curves, see Figure 4 (c) and (d). The $\Delta S(H)$ versus temperature relation is similar a to Gaussian curve, with a maximum $\Delta S(H)$ of 19.7 mK in FC and 20 mK in ZFC, which correspond to temperatures of 273 K and 273 K, respectively. Interestingly, the calculated MCE efficiency ($\Delta S(H)/\mu_0\Delta H$) in these heterostructures is found to be the higher than reported data for several LSMO based composition/configuration[11, 17-25]. $\Delta S(H)/\mu_0\Delta H$ could be considered as a criterion for comparing MCE efficiency in terms of per unit applied magnetic field. Here it is to be noted that some doped and strain engineered LSMO thin films grown under similar conditions shows higher MCE but only in a narrow temperature range[22, 25]. However, these multilayered structures are found to sustain this MCE over a broad temperature range (note the broad range of temperature corresponding to maximum entropy and temperature change in Figure 4). This profound the additional benefit of PZT/BSCCO layers and the possibility of utilizing them for better solid-state refrigeration devices.

4. Conclusions

In conclusion, present study elucidates the advantage of simultaneously exploiting magnetoelectric coupling and epitaxial strains effect for significant piezo- and magnetic response. In this context, multilayered heterostructures of $\text{PbZr}_{0.52}\text{Ti}_{0.48}\text{O}_3$ (PZT) (5 nm)/ Bi-Sr-Ca-Cu₂-O_x (BSCCO) (5 nm)/ $\text{La}_{0.67}\text{Sr}_{0.33}\text{MnO}_3$ (LSMO) (40 nm)/ MgO have been engineered to

have a strong magnetoelectric coupling and a strong magnetic response at room temperature. The same has been confirmed using a Field Cooled (FC) and Zero Field Cooled (ZFC) measurements which reveals these heterostructures as a potential candidate for MCE investigation. The MCE is calculated using Maxwell relations. Maximum entropy changes ($|\Delta S|$) of $42.6 \text{ mJkg}^{-1}\text{K}^{-1}$ and $41.7 \text{ mJkg}^{-1}\text{K}^{-1}$ are found for an applied magnetic field ($\mu_0\Delta H$) of 0.1 T corresponding to 258 K and 269 K, respectively. Moreover, $\Delta S(H)/\mu_0\Delta H$ values, which are often considered as a criterion for comparison of MCE refrigeration, in these heterostructures are also found to be significantly higher in contrast to several LSMO based compositions. Importantly, this MCE is found to sustain over a broad temperature range and thus profound the competency of engineered heterostructures for improved solid-state energy conversion devices. We sum up this study with a hope that this approach will motivate the research community for engineering similar heterostructures for better MCE.

References

- [1] V.K. Pecharsky, K.A. Gschneidner Jr, Giant magnetocaloric effect in Gd₅(Si₂Ge₂), Physical Review Letters, 78 (1997) 4494.
- [2] W. Giauque, D. MacDougall, Attainment of Temperatures Below 1° Absolute by Demagnetization of Gd₂(SO₄)₃·8H₂O, Physical Review, 43 (1933) 768.
- [3] T. Krenke, E. Duman, M. Acet, E.F. Wassermann, X. Moya, L. Mañosa, A. Planes, Inverse magnetocaloric effect in ferromagnetic Ni–Mn–Sn alloys, Nature materials, 4 (2005) 450-454.
- [4] O. Tegus, E. Brück, K. Buschow, F. De Boer, Transition-metal-based magnetic refrigerants for room-temperature applications, Nature, 415 (2002) 150-152.
- [5] J. Liu, T. Gottschall, K.P. Skokov, J.D. Moore, O. Gutfleisch, Giant magnetocaloric effect driven by structural transitions, Nature materials, 11 (2012) 620-626.
- [6] H. Zhu, C. Xiao, H. Cheng, F. Grote, X. Zhang, T. Yao, Z. Li, C. Wang, S. Wei, Y. Lei, Magnetocaloric effects in a freestanding and flexible graphene-based superlattice synthesized with a spatially confined reaction, Nature communications, 5 (2014).
- [7] F.-x. Hu, B.-g. Shen, J.-r. Sun, G.-h. Wu, Large magnetic entropy change in a Heusler alloy Ni_{52.6}Mn_{23.1}Ga_{24.3} single crystal, Physical Review B, 64 (2001) 132412.
- [8] V.K. Pecharsky, K.A. Gschneidner Jr, Tunable magnetic regenerator alloys with a giant magnetocaloric effect for magnetic refrigeration from 20 to 290K, Applied Physics Letters 70 (1997).

- [9] A. Fujita, S. Fujieda, Y. Hasegawa, K. Fukamichi, Itinerant-electron metamagnetic transition and large magnetocaloric effects in La (Fe x Si 1- x) 13 compounds and their hydrides, *Physical Review B*, 67 (2003) 104416.
- [10] X. Moya, L. Hueso, F. Maccherozzi, A. Tovstolytkin, D. Podyalovskii, C. Ducati, L. Phillips, M. Ghidini, O. Hovorka, A. Berger, Giant and reversible extrinsic magnetocaloric effects in La_{0.7}Ca_{0.3}MnO₃ films due to strain, *Nature materials*, 12 (2013) 52-58.
- [11] E. Brück, O. Tegus, D.C. Thanh, K. Buschow, Magnetocaloric refrigeration near room temperature, *Journal of Magnetism and Magnetic Materials*, 310 (2007) 2793-2799.
- [12] G. Jonker, J. Van Santen, Ferromagnetic compounds of manganese with perovskite structure, *physica*, 16 (1950) 337-349.
- [13] J. Van Santen, G. Jonker, Electrical conductivity of ferromagnetic compounds of manganese with perovskite structure, *Physica*, 16 (1950) 599-600.
- [14] G. Jonker, Magnetic compounds with perovskite structure IV conducting and non-conducting compounds, *Physica*, 22 (1956) 707-722.
- [15] J.-H. Park, E. Vescovo, H.-J. Kim, C. Kwon, R. Ramesh, T. Venkatesan, Direct evidence for a half-metallic ferromagnet, *Nature*, 392 (1998) 794-796.
- [16] A. Haghiri-Gosnet, J. Renard, CMR manganites: physics, thin films and devices, *Journal of Physics D: Applied Physics*, 36 (2003) R127.
- [17] B. Arayedh, S. Kallel, N. Kallel, O. Pena, Influence of non-magnetic and magnetic ions on the MagnetoCaloric properties of La_{0.7}Sr_{0.3}Mn_{0.9}M_{0.1}O₃ doped in the Mn sites by M= Cr, Sn, Ti, *Journal of Magnetism and Magnetic Materials*, 361 (2014) 68-73.
- [18] A. Rostamnejadi, M. Venkatesan, P. Kameli, H. Salamati, J. Coey, Magnetocaloric effect in La_{0.67}Sr_{0.33}MnO₃ manganite above room temperature, *Journal of Magnetism and Magnetic Materials*, 323 (2011) 2214-2218.
- [19] D. Nam, N. Dai, L. Hong, N. Phuc, S. Yu, M. Tachibana, E. Takayama-Muromachi, Room-temperature magnetocaloric effect in La_{0.7}Sr_{0.3}Mn_{1-x}Mx'O₃ (M'= Al, Ti), *Journal of Applied Physics*, 103 (2008) 043905.
- [20] W. Lu, X. Luo, C. Hao, W. Song, Y. Sun, Magnetocaloric effect and Griffiths-like phase in La_{0.67}Sr_{0.33}MnO₃ nanoparticles, *Journal of Applied Physics*, 104 (2008) 113908.
- [21] M.-H. Phan, H.-X. Peng, S.-C. Yu, N.D. Tho, N. Chau, Large magnetic entropy change in Cu-doped manganites, *Journal of Magnetism and Magnetic Materials*, 285 (2005) 199-203.
- [22] D.T. Morelli, A.M. Mance, J.V. Mantese, A.L. Micheli, Magnetocaloric properties of doped lanthanum manganite films, *Journal of applied physics*, 79 (1996) 373-375.
- [23] S. Chandra, A. Biswas, S. Datta, B. Ghosh, A. Raychaudhuri, H. Srikanth, Inverse magnetocaloric and exchange bias effects in single crystalline La_{0.5}Sr_{0.5}MnO₃ nanowires, *Nanotechnology*, 24 (2013) 505712.
- [24] Q. Zhang, S. Thota, F. Guillou, P. Padhan, V. Hardy, A. Wahl, W. Prellier, Magnetocaloric effect and improved relative cooling power in (La_{0.7}Sr_{0.3}MnO₃/SrRuO₃) superlattices, *Journal of Physics: Condensed Matter*, 23 (2011) 052201.
- [25] V.S. Kumar, R. Chukka, Z. Chen, P. Yang, L. Chen, Strain dependent magnetocaloric effect in La_{0.67}Sr_{0.33}MnO₃ thin-films, *AIP Advances*, 3 (2013) 052127.
- [26] H. Yang, Y. Zhu, T. Xian, J. Jiang, Synthesis and magnetocaloric properties of La_{0.7}Ca_{0.3}MnO₃ nanoparticles with different sizes, *Journal of Alloys and Compounds*, 555 (2013) 150-155.
- [27] B. Arayedh, S. Kallel, N. Kallel, O. Pena, Influence of non-magnetic and magnetic ions on the MagnetoCaloric properties of La_{0.7}Sr_{0.3}Mn_{0.9}M_{0.1}O₃ doped in the Mn sites by M= Cr, Sn, Ti, *Journal of Magnetism and Magnetic Materials*, 361 (2014) 68-73.

- [28] A. Kumar, D. Barrionuevo, N. Ortega, A. Shukla, S. Shannigrahi, J. Scott, R.S. Katiyar, Ferroelectric capped magnetization in multiferroic PZT/LSMO tunnel junctions, *Applied Physics Letters*, 106 (2015) 132901.
- [29] S. Thota, Q. Zhang, F. Guillou, U. Lüders, N. Barrier, W. Prellier, A. Wahl, P. Padhan, Anisotropic magnetocaloric effect in all-ferromagnetic (La_{0.7} Sr_{0.3} MnO₃/SrRuO₃) superlattices, *Applied Physics Letters*, 97 (2010) 112506.
- [30] G. Vats, A. Kumar, N. Ortega, C.R. Bowen, R.S. Katiyar, Pyroelectric control of magnetization for tuning thermomagnetic energy conversion and magnetocaloric effect, *Energy & environmental science*, 9 (2016) 2383-2391.
- [31] D. Pantel, H. Lu, S. Goetze, P. Werner, D. Jik Kim, A. Gruverman, D. Hesse, M. Alexe, Tunnel electroresistance in junctions with ultrathin ferroelectric Pb (Zr_{0.2}Ti_{0.8})O₃ barriers, *Applied Physics Letters*, 100 (2012) 232902.
- [32] D. Pantel, S. Goetze, D. Hesse, M. Alexe, Room-temperature ferroelectric resistive switching in ultrathin Pb (Zr_{0.2}Ti_{0.8})O₃ films, *ACS nano*, 5 (2011) 6032-6038.
- [33] E.Y. Tsymlal, H. Kohlstedt, Tunneling across a ferroelectric, Evgeny Tsymlal Publications, (2006) 22.
- [34] X. Ma, A. Kumar, S. Dussan, H. Zhai, F. Fang, H. Zhao, J. Scott, R. Katiyar, G. Lüpke, Charge control of antiferromagnetism at PbZr_{0.5}Ti_{0.48}O₃/La_{0.67}Sr_{0.33}MnO₃ interface, *Applied Physics Letters*, 104 (2014) 132905.
- [35] A. Crassous, R. Bernard, S. Fusil, K. Bouzouane, D. Le Bourdais, S. Enouz-Vedrenne, J. Briatico, M. Bibes, A. Barthélémy, J.E. Villegas, Nanoscale electrostatic manipulation of magnetic flux quanta in ferroelectric/superconductor BiFeO₃/YBa₂Cu₃O_{7- δ} heterostructures, *Physical review letters*, 107 (2011) 247002.
- [36] R.K. Rakshit, M. Singh, R. Katiyar, V. Ojha, A. Kumar, Tunneling current in magnetic-ferroelectric-superconducting heterostructures, *EPL (Europhysics Letters)*, 122 (2018) 57002.
- [37] J. Ma, J. Hu, Z. Li, C.W. Nan, Recent progress in multiferroic magnetoelectric composites: from bulk to thin films, *Advanced Materials*, 23 (2011) 1062-1087.
- [38] A. Brandlmaier, S. Geprägs, M. Weiler, A. Boger, M. Opel, H. Huebl, C. Bihler, M. Brandt, B. Botters, D. Grundler, In situ manipulation of magnetic anisotropy in magnetite thin films, *Physical Review B*, 77 (2008) 104445.
- [39] A. Visinoiu, R. Scholz, S. Chattopadhyay, M. Alexe, D. Hesse, Formation of epitaxial BaTiO₃/SrTiO₃ multilayers grown on Nb-doped SrTiO₃ (001) substrates, *Japanese journal of applied physics*, 41 (2002) 6633.
- [40] N. Ortega, A. Kumar, O. Maslova, Y.I. Yuzyuk, J. Scott, R. Katiyar, Effect of periodicity and composition in artificial BaTiO₃/(Ba, Sr)TiO₃ superlattices, *Physical Review B*, 83 (2011) 144108.
- [41] A. Kumar, S.G. Shivareddy, M. Correa, O. Resto, Y. Choi, M.T. Cole, R.S. Katiyar, J.F. Scott, G.A. Amaratunga, H. Lu, Ferroelectric-carbon nanotube memory devices, *Nanotechnology*, 23 (2012) 165702.
- [42] A. Gruverman, D. Wu, H. Lu, Y. Wang, H. Jang, C. Folkman, M.Y. Zhuravlev, D. Felker, M. Rzechowski, C.-B. Eom, Tunneling electroresistance effect in ferroelectric tunnel junctions at the nanoscale, *Nano letters*, 9 (2009) 3539-3543.
- [43] D.K. Pradhan, S. Kumari, E. Strelcov, D.K. Pradhan, R.S. Katiyar, S.V. Kalinin, N. Laanait, R.K. Vasudevan, Reconstructing phase diagrams from local measurements via Gaussian processes: mapping the temperature-composition space to confidence, *NPJ Computational Materials*, 4 (2018) 1-11.
- [44] A.M. Tishin, Y.I. Spichkin, *The magnetocaloric effect and its applications*, CRC Press, 2003.
- [45] J.S. Young, Indirect measurement of the electrocaloric effect, in, University of Cambridge, 2012.
- [46] G. Srinivasan, E. Rasmussen, B. Levin, R. Hayes, Magnetoelectric effects in bilayers and multilayers of magnetostrictive and piezoelectric perovskite oxides, *Physical Review B*, 65 (2002) 134402.

- [47] M. Bichurin, V. Petrov, G. Srinivasan, Theory of low-frequency magnetoelectric coupling in magnetostrictive-piezoelectric bilayers, *Physical Review B*, 68 (2003) 054402.
- [48] C. Kwon, M. Robson, K.-C. Kim, J. Gu, S. Lofland, S. Bhagat, Z. Trajanovic, M. Rajeswari, T. Venkatesan, A. Kratz, Stress-induced effects in epitaxial (La_{0.7}Sr_{0.3})MnO₃ films, *Journal of magnetism and magnetic materials*, 172 (1997) 229-236.
- [49] M. Saad, P. Baxter, R. Bowman, J. Gregg, F. Morrison, J. Scott, Intrinsic dielectric response in ferroelectric nano-capacitors, *Journal of Physics: Condensed Matter*, 16 (2004) L451.

Figure Captions

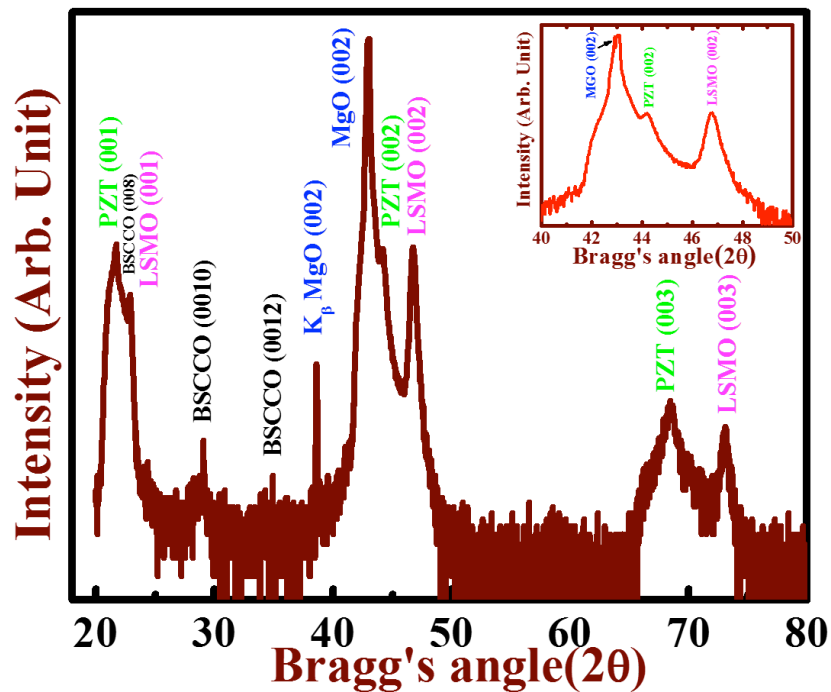


Figure 1: X-ray diffraction patterns of PZT/BSCCO/LSMO/MgO heterostructures, inset shows the slow scan XRD patterns between 40 to 50 degree Bragg's angles to view the highly oriented heterostructure

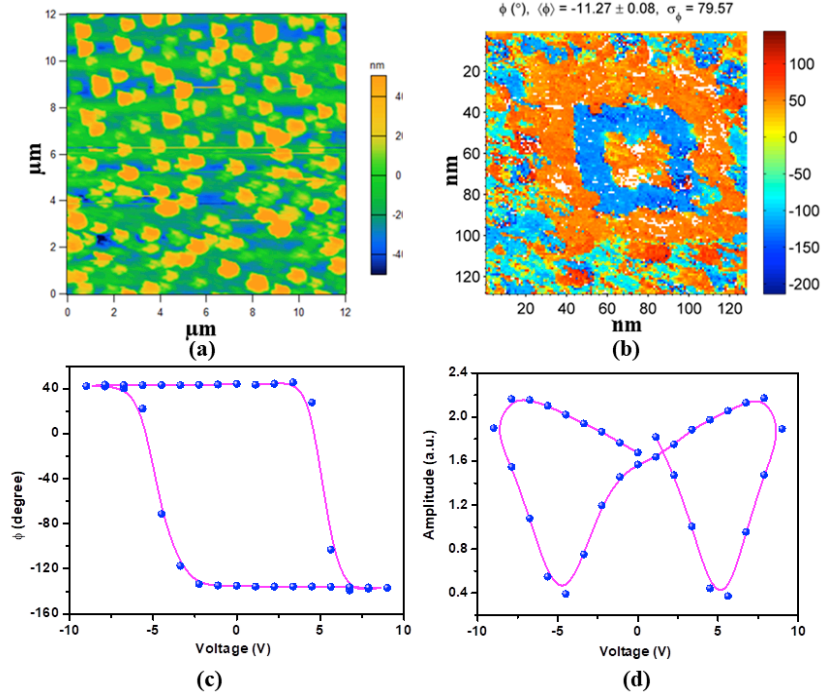


Figure 2: (a) Large area surface topography of PZT/BSCCO/LSMO/MgO heterostructures, (b) ferroelectric domain switching under external 8 V DC bias, (c) phase change and (d) variation in amplitude under applied external electric field.

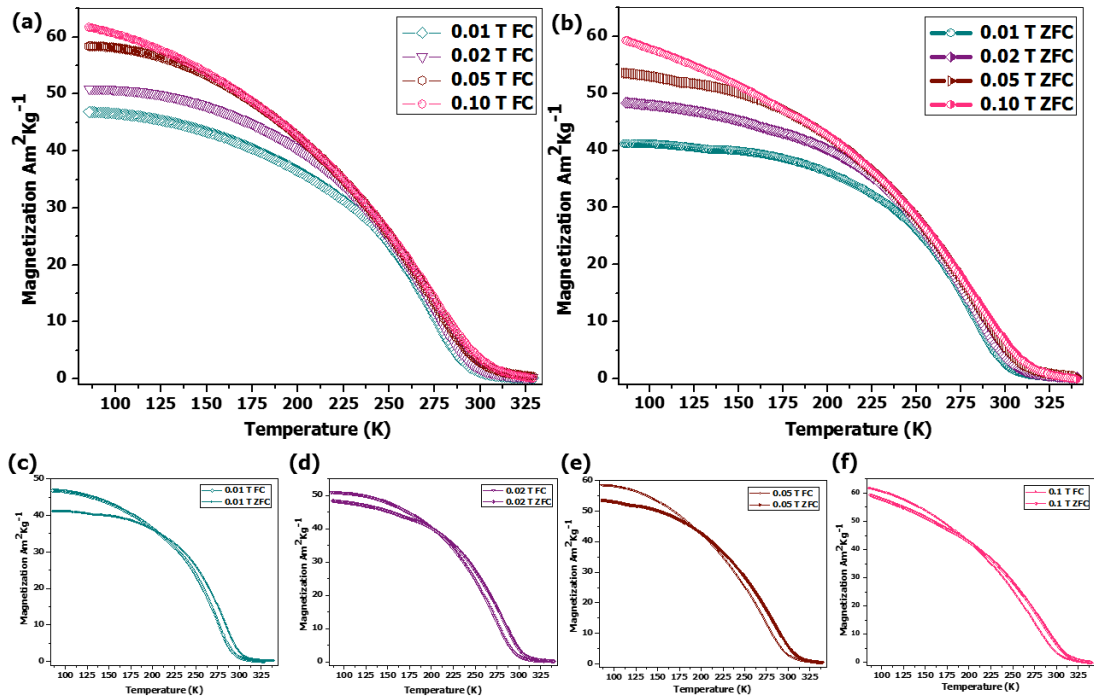


Figure 3: (a) Field Cooled (FC) and (b) Zero Field Cooled (ZFC) magnetization versus temperature plots ($M-T$) for PZT/BSCCO/LSMO/MgO heterostructures. (c)-(e) The variation in $M-T$ plots for 0.01 T, 0.02 T, 0.05 T and 0.1 T respectively.

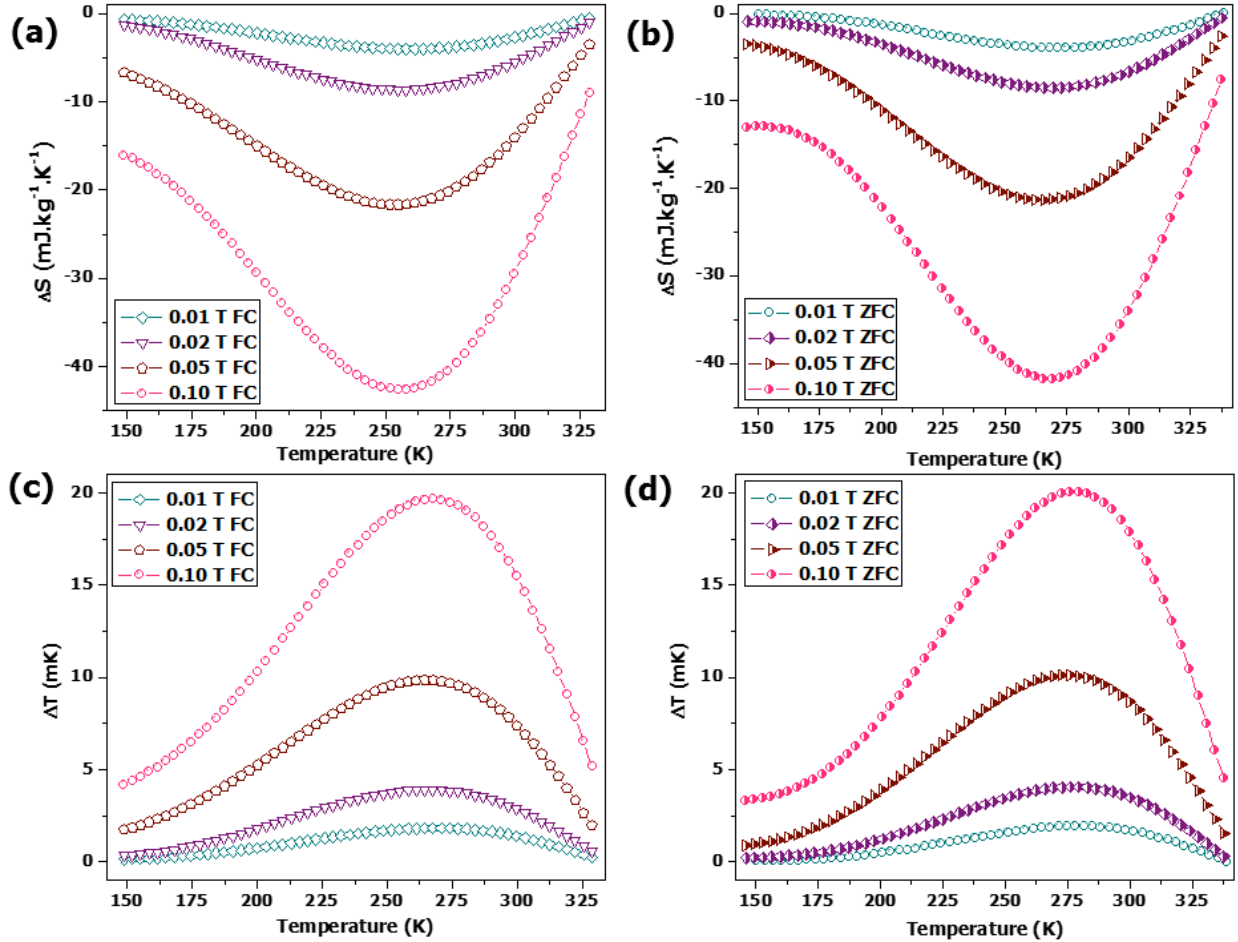


Figure 4: The variation in entropy (ΔS) as a function of temperature, calculated using Maxwell relations, for selected ranges of (a) Field Cooled (FC) and (b) Zero Field Cooled (ZFC) magnetic measurements. The corresponding temperature change (ΔT) as a function of temperature, calculated using Maxwell relations, for selected ranges of applied (c) Field Cooled (FC) and (d) Zero Field Cooled (ZFC) magnetic measurements.